Magnetic dichroisms in absorption and photoemission for magnetic characterization in x-ray photoelectron emission microscopy

W. Kuch,[a] L. I. Chelaru, F. Offi, M. Kotsugi, and J. Kirschner
Max-Planck-Institut für Mikrostrukturphysik, Weinberg 2, D-06120 Halle, Germany

(Received 13 May 2002; accepted 30 September 2002)

Magnetic contrast for the operation of a photoelectron emission microscope (PEEM) with synchrotron radiation is provided by magnetic dichroisms. Besides the most frequently employed magnetic dichroism, magnetic circular dichroism in x-ray absorption spectroscopy, energy filtering of photoemitted electrons allows one to also use magnetic dichroisms in photoelectron emission as complementary contrast mechanisms. We demonstrate that it is possible to obtain magnetic contrast in photoemission using PEEM equipped with a simple retarding field electron energy analyzer. Magnetic domain images of an ultrathin film of 10 atomic monolayers of Fe on W(001), obtained by three different contrast mechanisms (circular magnetic dichroism in x-ray absorption, circular magnetic dichroism in Fe valence band photoemission, and linear magnetic dichroism in Fe $3p$ photoemission) are presented and compared. © *2002 American Vacuum Society.*
[DOI: 10.1116/1.1523371]

I. INTRODUCTION

Imaging of magnetic domains has contributed greatly to our knowledge of micromagnetic phenomena.[1] Operation of a photoelectron emission microscope (PEEM) with synchrotron radiation offers unique possibilities for magnetic domain imaging.[2] The most frequently employed magnetic contrast mechanism for this technique is the x-ray magnetic circular dichroism (XMCD) which is observed in the absorption of soft x rays.[3,4] Due to excitation of spin-polarized electronic transitions from elemental core levels into the unoccupied spin–split valence states by circularly polarized x rays, the x-ray absorption and hence the total number of electrons emitted depends on the relative orientation of magnetization direction and the helicity of the x rays. This information is contained in the intensity of the total photoelectron yield, so that no energy filtering of the photoelectrons is necessary to observe the magnetic contrast. Further features of this method are the moderate surface or interface sensitivity, the possibility to use arbitrarily thick substrates including single crystals, and the element specificity of the observed magnetic information. The last especially is an invaluable advantage considering the complex magnetic multilayered systems and nanostructures which exhibit interesting phenomena such as giant magnetoresistance, spin-polarized tunneling, spin–torque transfer, or spin injection. PEEM in connection with XMCD has already been used successfully in a number of studies, for example, for layer-resolved imaging of noncollinear canted spin structures in Co/Cu/Ni trilayers.[5]

If energy filtering of photoemitted electrons is possible, magnetic dichroisms which occur in photoelectron spectroscopy may be employed as magnetic contrast mechanisms. Such dichroisms occur for various experimental geometries that involve circularly,[6–10] linearly,[10–19] or even unpolarized light,[20–27] and they can be observed in valence band[6,7,17–20,28] or core level photoemission spectra.[8–16,21–27] For highly symmetric geometries, circular dichroism in photoemission can be described in terms of relativistic selection rules for transitions between exchange and spin–orbit split states.[6,29] In most other cases magnetic dichroism in photoemission arises from interference between transition matrix elements for different polarization components.[29–32]

In contrast to magnetic circular dichroism in absorption, which (for fixed helicity) depends only on the relative orientation between the incidence of light and the magnetization direction, magnetic dichroism in photoemission depends on the relative orientation of three vectors. These are the direction of the incident x-ray beam, the magnetization direction, and the direction of the emitted electron. It is therefore also termed magnetic circular (MC) or magnetic linear (ML) dichroism (MCDAD or MLDAD) in the angular distribution of photoelectrons. Including the electron emission direction can induce a chirality in a geometry in which no dichroism would be observed in absorption; in such a geometry the magnetic dichroism would be averaged out in an angle-integrating photoemission experiment.[16,30] Angular resolution in photoelectron detection is thus necessary to observe this kind of dichroism.

To our knowledge, up to now magnetic dichroism in photoemission had been used in only two experiments as the contrast mechanism for imaging of magnetic domains. In a modified hemispherical electron energy analyzer with imaging capabilities circular magnetic dichroism in Fe $3p$ core level photoemission[33] and unpolarized magnetic dichroism in Fe $2p_{3/2}$ core level photoemission[34] had been used to obtain a magnetic domain image. Images in which linear magnetic dichroism in photoemission was the contrast mechanism have also been obtained from antiferromagnetic NiO using a scanning photoelectron microscope.[35] Here a focused x-ray beam was scanned across the sample, while Ni $3p$ photoelectrons were detected by a standard hemispherical electron energy analyzer. In both approaches the space between the sample and entrance lens of the spectrometer is essentially

[a]Electronic mail: kuch@mpi-halle.de

field free, and the bore of the electron optics defines the maximum acceptance angle. It was believed that with an immersion lens microscope like a PEEM, where a high electric field between the sample and the front of the first lens of the microscope accelerates the electrons, it would not be possible to employ these dichroisms as a magnetic contrast mechanism for imaging, since a large angular range of true starting angles at the sample is accelerated into the microscope. This is indeed true for the low-energy secondary electrons that mainly create the image in an unfiltered absorption experiment. For higher kinetic energies of emitted electrons, however, the contrast aperture that is positioned in the backfocal plane of the objective lens effectively limits the range of angles accepted. The maximum apparent starting angle α' ''seen'' by the instrument and the ''true'' starting angle α_0 of the electrons at the sample surface are related by the square root of the ratio of the energies as

$$\frac{\sin \alpha_0}{\sin \alpha'} = \sqrt{\frac{eU}{E_0} + 1}, \tag{1}$$

where E_0 is the true starting energy of the electrons, and U_{ex} is the accelerating voltage between sample and PEEM.[36] α' depends approximately linearly on the size of the aperture and on the geometry of the microscope. A typical value is $\alpha' = 3$ mrad. Using this value and $U_{\mathrm{ex}} = 15$ kV, the accepted starting angle at the sample is $\pm 31°$ for $E_0 = 0.5$ eV, but only $\pm 3°$ for $E_0 = 50$ eV. Thus, it may be possible, working in that range of kinetic energies, to use this angular resolution to get contrast from dichroisms in the angular distribution of photoelectrons.

In this article we report magnetic domain imaging using MCDAD and MLDAD as magnetic contrast mechanisms. This is to our knowledge the first observation of magnetic domains using dichroism in photoemission with an immersion lens microscope. We are able to obtain magnetic contrast in the Fe valence band (Fe $3d$) and in Fe $3p$ photoemission with a commercial PEEM equipped with a simple retarding grid high pass electron energy filter. Magnetic domain images of an ultrathin Fe film on a W(001) single crystal substrate obtained by ''conventional'' magnetic imaging using XMCD in absorption are compared to images obtained at the same positions by energy filtering photoemitted Fe $3d$ valence electrons and Fe $3p$ core electrons. These additional magnetic contrast mechanisms provide complementary information with respect to XMCD imaging: MLDAD using *p*-polarized excitation is sensitive to the transverse component of the magnetization vector, perpendicular to the light incidence azimuth, whereas XMCD only provides information about the longitudinal component, along the light incidence azimuth. Dichroism in valence band photoemission is sensitive to specific details of the electronic structure. In addition, varying the direction of linear polarization, sensitivity on the magnetization *axis*, not its direction, can be obtained, which may complement magnetic linear dichroism in absorption.[37]

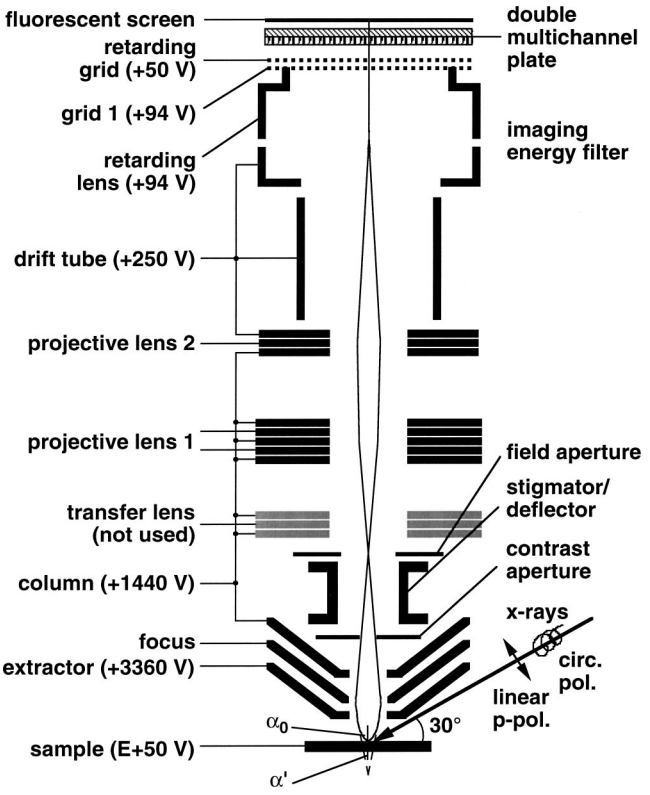

FIG. 1. Schematic of the setup of the PEEM. The sample is excited by circularly or linearly polarized x rays, incident 30° to the sample surface. The electrons emitted are accelerated towards the tetrode objective lens that consists of three elements (the extractor, focus, and column). Electron trajectories for electrons emitted from the sample by the maximum true starting angle α_0 are also shown. The corresponding maximum apparent starting angle α' is limited by the contrast aperture, located in the backfocal plane of the objective lens. An intermediate image is created in the plane of the field aperture, and further projected onto a fluorescent screen by a set of electrostatic lenses: the transfer lens (not used in the present work), a five-element and a three-element projective lens, and two lenses of the imaging energy filter. The voltages used in the present study are indicated. High pass energy filtering of the electrons at energy *E* is performed by the retarding grid of the imaging energy filter.

II. EXPERIMENT

The setup of our commercially available PEEM[38] is schematically depicted in Fig. 1. It is an all-electrostatic straight optical axis microscope with an integrated sample stage and a variable contrast aperture. The three element objective lens creates an image of the sample in the plane of the field aperture, which can be used to suppress stray electrons or to limit the field of view. An electrostatic octupole stigmator/deflector allows correction of astigmatism and alignment of the optical axis in any rotational direction.

For the measurements presented here the instrument was operated at an objective lens extraction voltage of 3.36 keV and a contrast aperture of 150 μm diameter in the backfocal plane of the objective lens. This resulted in $\alpha' = 5.3$ mrad and a spatial resolution of about 1 μm. Voltages of the two projective lenses were chosen to give a field of view of 155 μm. The relatively big aperture size and low extraction voltage were chosen in order to increase the image intensity, at the expense of lateral resolution. Note that approximately the

same angular electron acceptance would have been achieved if we had used a smaller aperture of the instrument (70 μm diameter) and maximum acceleration voltage of 15 kV [cf. Eq. (1)].

For energy analysis of the electrons, the instrument was equipped with an imaging energy filter[39] that consisted of two additional lenses and two grids, shown in Fig. 1, which are operated as a retarding field analyzer.[40] The voltages of the lenses are set to achieve normal incidence of the electrons on the grids, as schematically shown by the electron trajectories in Fig. 1. The retarding grid was kept at a constant potential of $+50$ V with respect to ground for the measurements presented here. For the energy scans the sample potential was scanned at $E+50$ V to obtain high pass images at energy E. Electrons emitted at that energy passed the PEEM electron optics at a column energy of 1390 eV, and were decelerated to 200 eV at projective lens 2 before entering the drift tube. In the imaging energy filter further deceleration by the retarding lens to 44 eV is achieved before the electrons pass the retarding grid at zero kinetic energy. With these settings an energy resolution of 0.6 eV was achieved, as is evident from the width of the cutoff in threshold photoemission spectra using a Hg discharge lamp. After intensification by a double multichannel plate, electron intensity images were recorded from a fluorescent screen by a charge coupled device camera[41] outside the vacuum. Binning of camera pixels corresponding to 775×775 nm^2 was used for the images presented here.

Our sample was an ultrathin Fe film on W(001),[42] grown by electron beam assisted thermal evaporation from high purity material at room temperature in ultrahigh vacuum (base pressure 1×10^{-8} Pa). The measurements presented here were obtained from Fe films of 10 atomic monolayer (ML) thickness. Synchrotron radiation from the helical undulator beamline UE56-2 PGM2 at BESSY II in Berlin was used, which was incident to the sample at an angle of 30° from the sample surface, as shown in Fig. 1, and 15° from the [010] azimuth. Linear or circular polarization could be selected by shifting the magnet structures of the undulator.[43]

III. RESULTS

Figure 2 shows a valence band photoemission spectrum for circularly σ^+-polarized light with photon energy $h\nu=122$ eV. The spectrum shown was calculated as the derivative of an energy series of high pass image intensities. While scanning the sample voltage, images were acquired with 10 s exposure time at each energy point. The photoemission spectrum displayed was obtained by averaging the electron intensity of these images over the whole field of view, and calculating the differences in intensity between adjacent energy steps. A broad maximum can be recognized between the Fermi edge and about 3 eV binding energy. It represents transitions from Fe valence states on the Δ axis with Δ^5 and Δ^1 symmetry into unoccupied states of Δ^1 symmetry.

In Fig. 3(a) we first show a magnetic domain image, obtained in the conventional way using XMCD in absorption. For this measurement the filter energy of the retarding field analyzer was set to zero and the photon energy to the maximum of the Fe L_3 absorption (707 eV). Here the image is mainly created by low energy secondary electrons, which are a measure of the local x-ray absorption. Figure 3(a) displays on a grayscale the intensity asymmetry of images acquired for opposite helicity of the circular polarization, defined as $[I_{\sigma^-}-I_{\sigma^+}]/[I_{\sigma^-}+I_{\sigma^+}]$. Different shades of gray correspond to different projections of the local magnetization direction onto the direction of the incoming light, which was from bottom to top in Fig. 3. The exposure time was 3 min for each helicity, and the grayscale of the image was adjusted to span 25% asymmetry. Domains of two different grayscale contrasts are observed. Quantitative analysis of the dichroic asymmetry in images for different sample azimuth angles reveals that in these domains the magnetization is along the

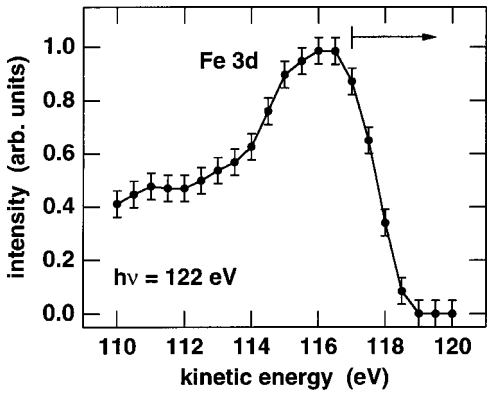

FIG. 2. Fe valence band photoemission spectrum of 10 ML Fe/W(001) for circularly σ^+-polarized excitation of 122 eV photon energy, acquired by high pass filtering in the PEEM by an imaging retarding field analyzer. The arrow marks the energy to which the analyzer was set for acquisition of the domain image in Fig. 3(b).

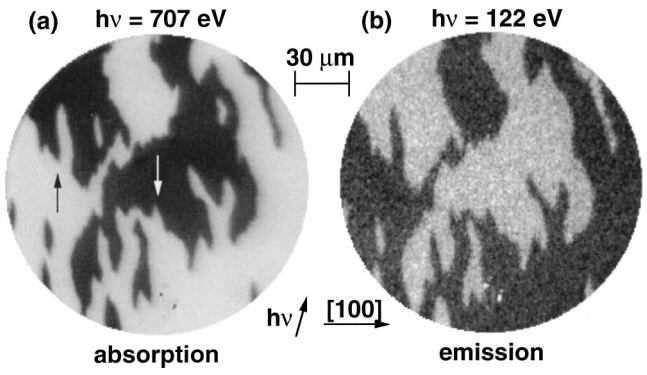

FIG. 3. (a) Magnetic domain image obtained by magnetic circular dichroism in absorption at the Fe L_3 absorption maximum (707 eV). No energy filtering of the electrons is performed here; high intensity low-energy secondary electrons carry information about the local absorption. White and black contrast corresponds to opposite magnetization directions along $\pm$[010] directions, indicated by arrows. (b) Photoemission intensity asymmetry image between images obtained with opposite helicity of circular polarization from photoelectrons of 117 eV kinetic energy or higher (cf. the arrow in Fig. 2), excited with 122 eV photon energy. The magnetic domain contrast in this image is due to the circular magnetic dichroism in valence band photoemission.

$\pm$[010] crystallographic directions of the W(001) substrate, as indicated by the arrows.

We now turn to MCDAD as the magnetic contrast mechanism. To do so, the photon energy is lowered to 122 eV, the same value for which the spectrum in Fig. 2 was recorded, and the high pass energy of the retarding field analyzer is set to 117 eV. The electrons that create the image are thus the photoelectrons from the high energy shoulder of the valence band peak, as indicated in Fig. 2 by an arrow. Figure 3(b) shows the intensity asymmetry upon helicity reversal under these conditions. Here the grayscale of the image spans 4.7% asymmetry and the acquisition time was 11 min for each helicity. The same domain pattern as that in Fig. 3(a) is clearly recognized, however with reverse contrast. Minor differences in small domain details in Fig. 3(b), which was acquired about 2.5 h after acquisition of Fig. 3(a) and about 7 h after film preparation, are due to coarsening of the domains, which obviously was still a slow ongoing process at room temperature. One such detail is the disappearance of two small islanded white domains that are visible in Fig. 3(a).

In the present geometry, in which circularly polarized light is incident in the plane defined by the magnetization and the sample normal, MCDAD in valence band photoemission is caused by interference between matrix elements of the electric field vector parallel and perpendicular to the surface.[28,29] In Fe(001), the former component of light polarization excites only transitions from states with Δ^5 symmetry, the latter only transitions from states with Δ^1 symmetry. Dichroism is thus observed only in regions in which Δ^1 and Δ^5 bands are sufficiently hybridized. Along the [001] direction in bulk Fe, such hybridization occurs where the *d*-like Δ^5 minority band and an *sp*-like Δ^1 majority band cross just below the Fermi edge at about 30% $\overline{\Gamma H}$.[44] We conclude that photoemission from this region in *k* space is responsible for the observed dichroism, and that the symmetry properties of these bands give rise to the reverse contrast with respect to the XMCD image in Fig. 3(a).

A photoemission spectrum of the Fe 3*p* region, obtained with linearly *p*-polarized light of 122 eV photon energy, is presented in Fig. 4. Again PEEM and a retarding field analyzer have been used as the photoelectron detector, like what was described above in connection with Fig. 2. The Fe 3*p* photoemission peak can be recognized at an electron energy of 64 eV.

MLDAD in Fe 3*p* photoemission with *p*-polarized excitation shows up as a plus/minus difference in intensity almost symmetric to the center of the peak.[10–15] In order to make local MLDAD differences visible, high pass images were acquired at 62, 64, and 66 eV electron energy. Here the total acquisition time of each of these images was 25 min. The differences between the images represent the photoemission intensity in two 2 eV intervals from 62 to 64 eV, and from 64 to 66 eV, labeled ''a'' and ''b'' in Fig. 4, respectively. Linear magnetic dichroism is thus expected to show up as intensity asymmetry between intensities ''a'' and ''b.''

In Fig. 5(a) we first show a conventional domain image of

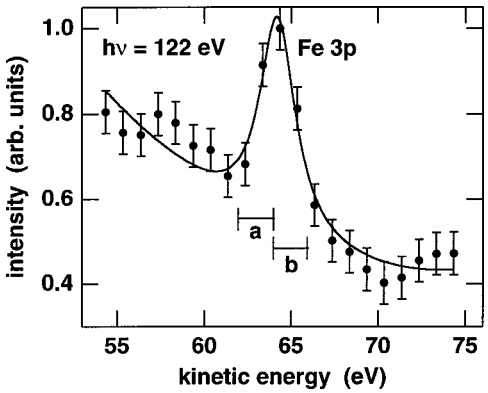

FIG. 4. Fe 3*p* photoemission spectrum of 10 ML Fe/W(001) for linearly *p*-polarized excitation of 122 eV photon energy, acquired by high pass filtering in the PEEM by an imaging retarding field analyzer. ''a'' and ''b'' mark the regions where linear magnetic dichroism in photoemission is expected. The solid line is a guide to the eye.

the Fe film using XMCD in absorption as the magnetic contrast mechanism. The photon energy was tuned to 707 eV, the maximum of the Fe L_3 absorption line, and no energy filtering of the photoelectrons was performed here. The grayscale of the image was adjusted to span 25% asymmetry. A magnetization pattern with three different domains is observed, characterized by white, black, and gray contrast. Quantitative analysis of the dichroic asymmetry reveals that the magnetization in these domains is along $\langle 100 \rangle$ in-plane crystallographic directions of the W(001) substrate, as indicated by arrows.

Having established the magnetic domain configuration, we now turn to the image obtained by MLDAD contrast in Fe 3*p* photoemission. Figure 5(b) shows the photoemission intensity asymmetry between energy regions ''a'' and ''b,'' defined as $(I_a - I_b)/(I_a + I_b)$. The grayscale of the image again spans 25% of this asymmetry, like that for the circular dichroic asymmetry of Fig. 5(a). The same domain pattern as

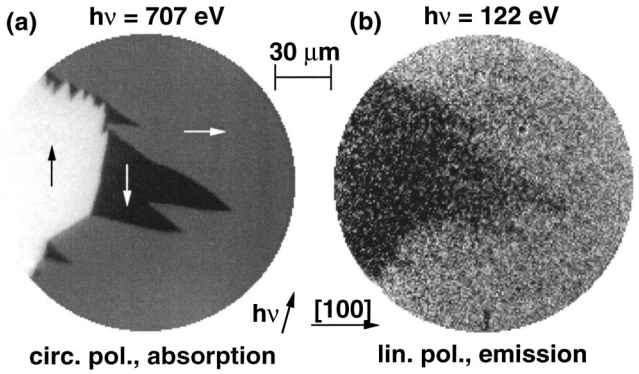

FIG. 5. (a) Magnetic domain image obtained by magnetic circular dichroism in absorption at the Fe L_3 absorption maximum (707 ev). White, black, and gray contrast levels correspond to three different magnetization directions along the substrate $\langle 100 \rangle$ directions, indicated by arrows. (b) Photoemission intensity asymmetry image between intensities obtained in energy regions ''a'' and ''b'' in Fig. 4 for *p*-polarized excitation of 122 eV photon energy. The magnetic domain contrast in this image is due to linear magnetic dichroism in Fe 3*p* core level photoemission.

that in Fig. 5(a) can be recognized, however with different relative contrast. The black and white domains of Fig. 5(a) now exhibit similar dark contrast, whereas the surrounding area (magnetization pointing toward the right) appears brighter. This is a consequence of the angular dependence of MLDAD,[11,12,16,29–32] where the contrast between opposite magnetization directions in the plane of light incidence and polarization axis vanishes. In this geometry MLDAD is sensitive to the transverse component of the magnetization, leading to the observed contrast between the brighter area (transverse component pointing toward the right) and the darker area (transverse component close to zero). A small difference in grayscale contrast between the domains that are black and white in Fig. 5(a) is faintly visible also in Fig. 5(b), but with reversed sign; this is due to the not completely vanishing transverse component in these domains with respect to the light incidence direction, which was 15° from the [010] direction, as indicated by the arrow labeled "$h\nu$." A domain with a transverse component pointing toward the left, which unfortunately could not be found in the present sample, would lead to even darker contrast.

IV. DISCUSSION

The possibility of exploiting magnetic dichroisms in photoemission opens up new sources of information on the magnetic properties of a sample. The most prominent one is the sensitivity of MLDAD on the transverse component of the magnetization, well known from numerous photoemission experiments.[11–28] This is even true for excitation by circularly polarized light,[7] where the intensity asymmetry for different kinetic energies depends on both the longitudinal and the transverse components. This is due to the fact that for circular polarization a mixture of two effects contributes to this asymmetry,[28–32] one being the linear dichroism displayed in Fig. 5(b), since circularly polarized light can be regarded as a coherent superposition of *s*- and *p*-polarized light. The other effect probes the longitudinal magnetization direction, and leads also to dichroism if one keeps the electron energy constant and reverses the helicity.

Magnetic dichroism in valence band photoemission depends sensitively on details of the electronic band structure, which are influenced by structural modifications such as strain and lattice deformation (for a recent review about magnetic dichroism in valence band photoemission, see Ref. 28, and references therein). This mechanism can therefore be used to obtain magnetic domain images on an electronic or even structural basis.

Another point is the additional information gained by the different depth sensitivity of XMCD and MCDAD or MLDAD. Relevant depth information in photoemission is the elastic mean free path of the photoelectrons.[45] If x-ray absorption is measured by secondary electron yield, the relevant length is the mean free path of inelastically scattered electrons, which is typically a factor of 2 higher than the elastic mean free path.[46] This can be helpful, for example, to distinguish contributions by moments induced at the upper and lower interfaces of a nonferromagnetic spacer layer sandwiched between two ferromagnetic layers.[47–49]

There is no dichroism upon magnetization reversal if *s*- instead of *p*-polarized x rays are used.[11,12,29–32] There is, however, a dichroism that shows up for 90° rotation of the magnetization.[12] This dichroism is thus sensitive to the *axis* of the magnetization. It has been shown that for *p*-polarized light also a dichroism between magnetization averaged spectra can be observed.[14] Spectra in which the magnetization is averaged over the two opposite magnetization directions parallel to light polarization are different from those averaged over the two opposite magnetization directions perpendicular to light polarization.[14] Such sensitivity on the magnetization *axis* instead of on the magnetization direction may be used to study domains in collinear antiferromagnets. An initial attempt to image antiferromagnetic domains in NiO films on Ag(001) using MLDAD in a scanning photoemission microscope was reported by Spanke *et al.*[35] Recently Stöhr and co-workers succeeded in imaging antiferromagnetic domains in oxide samples using XMLD in absorption.[50,51] This has received considerable attention because of the renewed interest in antiferromagnetic materials due to their use in magnetoresistive devices.[52] The contrast in XMLD relies on the shift of x-ray absorption intensity between the two crystal field-split peaks at the L_2 edge in oxides.[37] This effect is proportional to the square of the magnetization vector, so it also depends on the axial orientation of antiferromagnetic spins with respect to the light polarization axis. In metallic materials, however, it almost vanishes due to the vanishing crystal field splitting of the absorption peaks, leaving only an extremely small effect. Attempts to image domains in metallic antiferromagnets like, for example, in the technologically relevant materials IrMn and FeMn, have been unsuccessful so far. The above mentioned linear dichroisms in photoemission, on the other hand, have been demonstrated using metallic samples, and hence could constitute an alternative mechanism for the imaging of antiferromagnetic domains in metallic antiferromagnets.

Although the asymmetry of XMCD and MLDAD is of the same order [cf. Figs. 5(a) and 5(b), respectively], there is clearly more noise in Fig. 5(b). The main reason is that in using MLDAD in photoemission only the photoelectrons within a certain energy interval, in our case the intervals labeled "a" and "b" in Fig. 4, are used for imaging. They constitute only a very small fraction of the total photoelectron current, which is dominated by low-energy secondary electrons. In absorption images, such as those in Fig. 5(a), in which no energy filtering is performed, the electron intensity is more than two orders of magnitude higher. It is mainly just this difference in intensity that makes up for the worse statistics of Fig. 5(b).

Since MLDAD requires the interference of matrix elements, it depends on the electronic band structure, and is prominently observed only at certain photon energies.[10,15] It is, however, not necessary to tune the photon energy exactly to an absorption edge of a certain element, so it should be also observable with laboratory excitation sources. Tuning

the photon energy to a maximum of the effect, on the other hand, could improve the image quality. In addition, photoelectron diffraction effects impose a strong dependence on the photon energy, but in particular also on the electron emission angle with respect to the surface normal for fixed angle between light incidence and electron emission.[22–26] These effects can enhance the dichroism at emission angles a few degrees off the surface normal by a factor of up to 4 compared to normal emission.[23] Positioning the aperture off the optical axis in a certain direction in order to detect this off-normal photoemission could therefore be used to further enhance dichroic contrast.

In the present case a simple add-on energy filter was used on a PEEM that is normally mainly applied for magnetic imaging by magnetic dichroism in absorption. This has the great advantage that by simply switching the energy filter on and off it is possible to obtain magnetic contrast from different mechanisms, as was demonstrated. By using more sophisticated imaging energy filters with higher efficiency[53–55] it will be possible to routinely use magnetic dichroism in photoemission for magnetic domain imaging. The simple retarding field analyzer used in the present experiment has an advantage when the photoemission intensity close to the Fermi energy is used for imaging. The cutoff at the Fermi edge then acts as the corresponding low pass filter, so no subtraction of images is required in that case.

V. CONCLUSION

We have demonstrated that by energy filtering of the electrons that are used for creating the image of the sample in a photoemission microscope it is possible to obtain magnetic domain images in off-resonant excitation conditions. In this case magnetic dichroisms in photoemission are the mechanisms that provide magnetic contrast. They can complement information obtained by x-ray magnetic circular dichroism in absorption in many ways. In the examples presented here the use of a simple add-on retarding field analyzer was sufficient to observe magnetic domain contrast from circular dichroism in Fe valence band photoemission and from linear dichroism in Fe $3p$ core level photoemission. Looking toward the future, exploiting magnetic linear dichroism in photoemission may even be useful for imaging antiferromagnetic domains in metallic systems.

ACKNOWLEDGMENTS

The authors thank B. Zada and W. Mahler for technical assistance, M. Merkel and M. Escher for help and valuable suggestions, and the BESSY staff for help and for continuing support during beam times. Financial support by the German Minister for Education and Research (BMBF) under Grant Nos. 05 SL8EF19 and 05 KS1EFA6 is gratefully acknowledged.

[1]See, for example, A. Hubert and R. Schäfer, *Magnetic Domains* (Springer, Berlin, 1998).
[2]J. Stöhr, Y. Wu, M. G. Samant, B. B. Hermsmeier, G. Harp, S. Koranda, D. Dunham, and B. P. Tonner, Science **259**, 658 (1993).
[3]G. Schütz, W. Wagner, W. Wilhelm, P. Kienle, R. Zeller, R. Frahm, and G. Materlik, Phys. Rev. Lett. **58**, 737 (1987).
[4]J. Stöhr, J. Electron Spectrosc. Relat. Phenom. **75**, 253 (1995).
[5]W. Kuch, X. Gao, and J. Kirschner, Phys. Rev. B **65**, 064406 (2002).
[6]W. Kuch, A. Dittschar, K. Meinel, M. Zharnikov, C. M. Schneider, J. Kirschner, J. Henk, and R. Feder, Phys. Rev. B **53**, 11621 (1996).
[7]D. Venus, Phys. Rev. B **56**, 2661 (1997).
[8]L. Baumgarten, C. M. Schneider, H. Petersen, F. Schäfers, and J. Kirschner, Phys. Rev. Lett. **65**, 492 (1990).
[9]F. U. Hillebrecht, Ch. Roth, H. B. Rose, M. Finazzi, and L. Braicovich, Phys. Rev. B **51**, 9333 (1995).
[10]J. Bansmann, L. Lu, K. H. Meiwes-Broer, T. Schlathölter, and J. Braun, Phys. Rev. B **60**, 13860 (1999).
[11]Ch. Roth, F. U. Hillebrecht, H. B. Rose, and E. Kisker, Phys. Rev. Lett. **70**, 3479 (1993).
[12]Ch. Roth, H. B. Rose, F. U. Hillebrecht, and E. Kisker, Solid State Commun. **86**, 647 (1993).
[13]F. Sirotti and G. Rossi, Phys. Rev. B **49**, 15682 (1994).
[14]G. Rossi, G. Panaccione, F. Sirotti, and N. A. Cherepkov, Phys. Rev. B **55**, 11483 (1997).
[15]G. Panaccione, F. Sirotti, and G. Rossi, Solid State Commun. **113**, 373 (2000).
[16]W. Kuch, M.-T. Lin, W. Steinhögl, C. M. Schneider, D. Venus, and J. Kirschner, Phys. Rev. B **51**, 609 (1995).
[17]H. B. Rose, Ch. Roth, F. U. Hillebrecht, and E. Kisker, Solid State Commun. **91**, 129 (1994).
[18]D. Venus, W. Kuch, M.-T. Lin, C. M. Schneider, H. Ebert, and J. Kirschner, Phys. Rev. B **55**, 2594 (1997).
[19]A. Rampe, G. Güntherodt, D. Hartmann, J. Henk, T. Scheunemann, and R. Feder, Phys. Rev. B **57**, 14370 (1998).
[20]M. Getzlaff, Ch. Ostertag, G. H. Fecher, N. A. Cherepkov, and G. Schönhense, Phys. Rev. Lett. **73**, 3030 (1994).
[21]F. U. Hillebrecht and W.-D. Herberg, Z. Phys. B: Condens. Matter **93**, 299 (1994).
[22]A. Fanelsa, R. Schellenberg, F. U. Hillebrecht, E. Kisker, J. G. Menchero, A. P. Kaduwela, C. S. Fadley, and M. A. Van Hove, Phys. Rev. B **54**, 17962 (1996).
[23]R. Schellenberg, E. Kisker, M. Faust, A. Fanelsa, and F. U. Hillebrecht, Phys. Rev. B **58**, 81 (1998).
[24]R. Schellenberg, E. Kisker, A. Fanelsa, F. U. Hillebrecht, J. G. Menchero, A. P. Kaduwela, C. S. Fadley, and M. A. Van Hove, Phys. Rev. B **57**, 14310 (1998).
[25]X. Gao, M. Salvietti, W. Kuch, C. M. Schneider, and J. Kirschner, Phys. Rev. B **58**, 15426 (1998).
[26]X. Gao, M. Salvietti, W. Kuch, C. M. Schneider, and J. Kirschner, J. Electron Spectrosc. Relat. Phenom. **113**, 137 (2001).
[27]C. M. Schneider, U. Pracht, W. Kuch, A. Chassé, and J. Kirschner, Phys. Rev. B **54**, R15618 (1996).
[28]W. Kuch and C. M. Schneider, Rep. Prog. Phys. **64**, 147 (2001).
[29]J. Henk, T. Scheunemann, S. V. Halilov, and R. Feder, J. Phys.: Condens. Matter **8**, 47 (1996).
[30]D. Venus, Phys. Rev. B **48**, 6144 (1993); **49**, 8821 (1994).
[31]N. A. Cherepkov, Phys. Rev. B **50**, 13813 (1994).
[32]B. T. Thole and G. van der Laan, Phys. Rev. B **49**, 9613 (1994).
[33]C. M. Schneider, Z. Celinski, M. Neuber, C. Wilde, M. Grunze, K. Meinel, and J. Kirschner, J. Phys.: Condens. Matter **6**, 1177 (1994).
[34]C. M. Schneider, J. Magn. Magn. Mater. **175**, 160 (1997), Fig. 10.
[35]D. Spanke, V. Solinus, D. Knabben, F. U. Hillebrecht, F. Ciccacci, L. Gregoratti, and M. Marsi, Phys. Rev. B **58**, 5201 (1998).
[36]G. Schönhense, J. Phys.: Condens. Matter **11**, 9517 (1999).
[37]D. Alders, L. H. Tjeng, F. C. Voogt, T. Hibma, G. A. Sawatzky, C. T. Chen, J. Vogel, M. Sacchi, and S. Iacobucci, Phys. Rev. B **57**, 11623 (1998).
[38]Focus IS PEEM (Omicron).
[39]Focus imaging energy filter (Omicron).
[40]M. Merkel, M. Escher, J. Settemeyer, D. Funnemann, A. Oelsner, Ch. Ziethen, O. Schmidt, M. Klais, and G. Schönhense, Surf. Sci. **480**, 196 (2001).
[41]PCO SensiCam.
[42]W. Wulfhekel, F. Zavaliche, F. Porrati, H. P. Oepen, and J. Kirschner, Europhys. Lett. **49**, 651 (2000).
[43]M. R. Weiss *et al.*, Nucl. Instrum. Methods Phys. Res. A **467–468**, 449 (2001).

[44]C. S. Wang and J. Callaway, Phys. Rev. B **16**, 2095 (1977).
[45]M. P. Seah and W. A. Dench, Surf. Interface Anal. **1**, 2 (1979).
[46]R. Nakajima, J. Stöhr, and Y. U. Idzerda, Phys. Rev. B **59**, 6421 (1999).
[47]M. G. Samant *et al.*, Phys. Rev. Lett. **72**, 1112 (1994).
[48]W. Kuch, M. Salvietti, X. Gao, M.-T. Lin, M. Klaua, J. Barthel, C. V. Mohan, and J. Kirschner, Phys. Rev. B **58**, 8556 (1998).
[49]A. Scherz, H. Wende, P. Poulopoulos, J. Lindner, K. Baberschke, P. Blomquist, R. Wäppling, F. Wilhelm, and N. B. Brookes, Phys. Rev. B **64**, 180407 (2001).
[50]A. Scholl *et al.*, Science **287**, 1014 (2000).
[51]J. Stöhr, A. Scholl, T. J. Regan, S. Anders, J. Lüning, M. R. Scheinfein, H. A. Padmore, and R. L. White, Phys. Rev. Lett. **83**, 1862 (1999).
[52]C. H. Tsang, R. E. Fontana, Jr., T. Lin, D. E. Heim, B. A. Gurney, and M. L. Williams, IBM J. Res. Dev. **42**, 103 (1998).
[53]R. Fink *et al.*, J. Electron Spectrosc. Relat. Phenom. **84**, 231 (1997).
[54]Y. Sakai, M. Kato, S. Masuda, Y. Harada, and T. Ichinokawa, Surf. Rev. Lett. **5**, 1199 (1998).
[55]Th. Schmidt, S. Heun, J. Slezak, J. Diaz, K. C. Prince, G. Lilienkamp, and E. Bauer, Surf. Rev. Lett. **5**, 1287 (1998).